Experimental Determination of the Energy per Particle in Partially Filled Landau Levels

Fangyuan Yang, Alexander A. Zibrov, Ruiheng Bai, Takashi Taniguchi, Kenji Watanabe, Michael P. Zaletel, and Andrea F. Young

Phys. Rev. Lett. **126**, 156802 — Published 13 April 2021

DOI: 10.1103/PhysRevLett.126.156802

Experimental determination of the energy per particle in partially filled Landau levels

Fangyuan Yang,[1] Alexander A. Zibrov,[1] Ruiheng Bai,[1] Takashi Taniguchi,[2]
Kenji Watanabe,[3] Michael P. Zaletel,[4] and Andrea F. Young[1,*]

[1]*Department of Physics, University of California at Santa Barbara, Santa Barbara CA 93106, USA*
[2]*International Center for Materials Nanoarchitectonics, National Institute for Materials Science, 1-1 Namiki, Tsukuba 305-0044, Japan*
[3]*Research Center for Functional Materials, National Institute for Materials Science, 1-1 Namiki, Tsukuba 305-0044, Japan*
[4]*Department of Physics, University of California, Berkeley, CA 94720 USA*

(Dated: January 27, 2021)

We describe an experimental technique to measure the chemical potential, μ, in atomically thin layered materials with high sensitivity and in the static limit. We apply the technique to a high quality graphene monolayer to map out the evolution of μ with carrier density throughout the N=0 and N=1 Landau levels at high magnetic field. By integrating μ over filling factor, ν, we obtain the ground state energy per particle, which can be directly compared with numerical calculations. In the N=0 Landau level, our data show exceptional agreement with numerical calculations over the whole Landau level without adjustable parameters, as long as the screening of the Coulomb interaction by the filled Landau levels is accounted for. In the N=1 Landau level, comparison between experimental and numerical data suggests the importance of valley anisotropic interactions and reveals a possible presence of valley-textured electron solids near odd filling.

Partially filled Landau levels (LLs) are a paradigmatic example of flat band systems where dominant Coulomb interactions lead to a rich phase diagram of correlation driven electron states. Theoretically, the partially filled LL provides a compromise between phenomenological richness and computational tractability. However, quantitatively benchmarking numerical methods with transport measurements is typically limited to a discrete set of LL filling factors, ν. Thermodynamic quantities such as the chemical potential μ are more closely related to theoretically calculable quantities. Owing to recent progress in improving sample quality[1] and the fact that the single particle band structure is known to a high degree of accuracy, graphene is an ideal venue to pursue quantitative understanding of partially filled LLs. In this Letter we report precise measurements of μ in a high quality monolayer graphene layer at both zero and high magnetic fields. Typical measurements of thermodynamic quantities in graphene probe the compressibility $\partial n/\partial\mu$ at finite frequency[2–5], hindering accurate measurements in the quantum Hall regime where equilibration times can become long. Our measurements probe μ directly[6] in the static, $\omega \to 0$ limit. This allows us to determine μ across a continuous range of ν, and subsequently the total energy per flux quantum, E, where $\mu = \partial E/\partial\nu$.

Our heterostructure consists of two graphene monolayers embedded between top and bottom graphite gates (see Figs. 1a-b and S1), with each conducting layer separated by a hexagonal boron nitride (hBN) dielectric of approximately 40nm thickness. The dual graphite-gated structure ensures low charge inhomogeneity on both graphene monolayers while allowing independent control of their respective carrier densities through the static gate voltages applied to the top gate (v_t), bottom gate (v_b), and top monolayer (v_d). Internal contacts[12–16] are attached to the top monolayer—designated the 'detector'—and are used to measure its bulk conductivity σ_d. To measure μ of the bottom ('sample') graphene, we keep it grounded, and control μ by sweeping v_b. For each fixed v_b, we adjust the v_t to null the effect of changes in μ on the on the detector layer density. Under these conditions, the change in detector layer density $\delta n_d = 0$, which implies $\delta\mu = -c_t\delta v_t/c_0$[17]. $\delta\mu$ is then determined by recording δv_t, and calibrating the geometric capacitance lever arm c_t/c_0 (see Fig. S2).

Functionally, $\delta n_d = 0$ is enforced by choosing a "target" density n_d such that σ_d is at a conductance minimum corresponding to the Dirac point at B=0T or a weak FQH state at high B. Figure 1b shows the schematic of our measurement circuit which uses a digital feedback loop to maintain σ_d at its minimum as other parameters are swept. While the current measurement is done at finite frequency to allow low noise readout, it does not require charging of the sample layer at these frequencies. This allows us to access regimes where the sample layer conductivity is very small and equilibration times are very large. In practice, measurements are typically done with equilibration times of $\tau \approx 1$ sec.

Fig. 1d shows μ measured at B=0T and 200mT, plotted as a function of the sample carrier density $n = c_0(v_d - \mu) + c_b(v_b - \mu)$, where c_b is the capacitance between the sample and the bottom gate. $\mu(n)$ shows the $\sqrt{n}$ dependence expected for the linearly dispersing bands of monolayer graphene[2], as well as steps associated with LL formation when a small magnetic field is applied. To quantitatively model the data, we take $\mu^2 = (\Delta_{AB}/2)^2 + (\hbar v_F\sqrt{\pi|n|})^2$, where Δ_{AB} is the sublattice splitting that most arises due to alignment of the graphene with one of the encapsulating hBN layers [7, 8] and v_F is the Fermi velocity. We determine

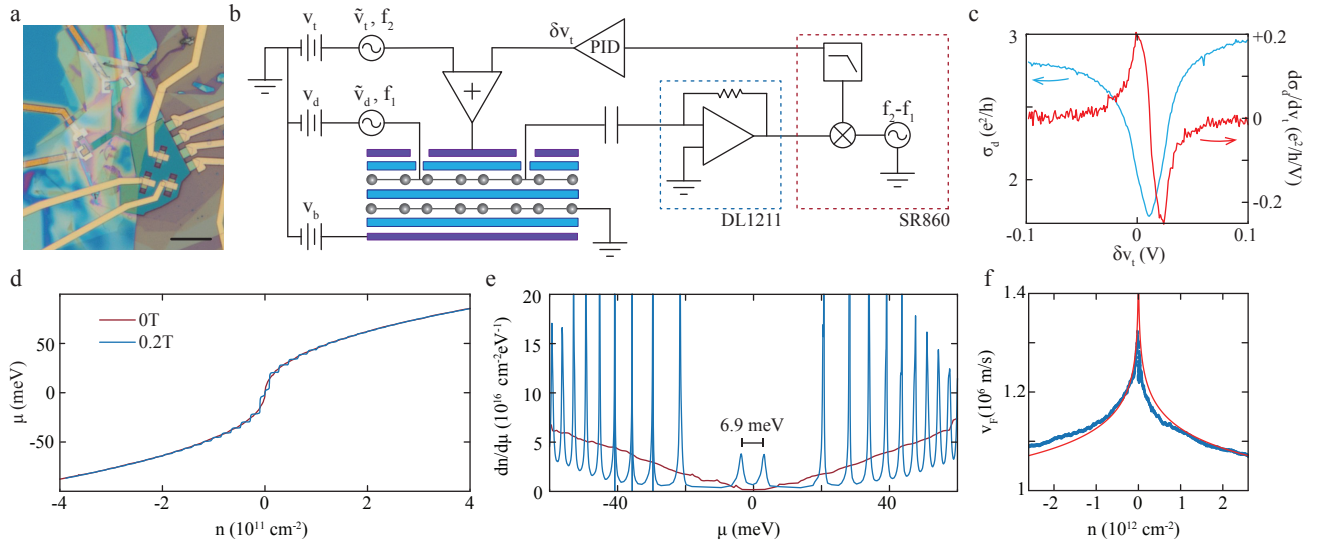

FIG. 1. **(a)** Optical image of the device, scale bar is 10μm. **(b)** Measurement schematic. Static gate voltages are applied to the top gate (v_t), bottom gate (v_b), and detector monolayer (v_d). σ_d is measured by applying an AC voltage $\tilde{v}_d$ at frequency $f_1 = 13.77$Hz to one of the internal contacts and measuring the current at another with a DL1211 amplifier. An additional AC voltage ($\tilde{v}_t$) is applied to the top gate at $f_2 = 110$Hz. Demodulating the current at $f_2 - f_1$ with an SR860 lock-in amplifier produces a signal proportional to $d\sigma_d/dv_t$, which vanishes at a conductivity minimum independent of contact resistance. We use a feedback loop to continuously adjust a static voltage δv_t in order to maintain $d\sigma_d/dv_t = 0$. Under these conditions, $\delta\mu = -c_t\delta v_t/c_0$. **(c)** σ_d (blue) and $\delta\sigma_d/\delta v_t$ (red) as a function of δv_t. **(d)** $\mu(n)$ at B=0T (red) and 0.2T (blue), measured at T=15mK. **(e)** Density of states $dn/d\mu$ calculated by numerical differentiation of data in panel (d). The ZLL is split by a sublattice gap[7, 8] of $\Delta_{AB} = 6.9$meV. **(f)** n-dependent v_F measured by fitting B=0T data to $\mu^2 = (\Delta_{AB}/2)^2 + (\hbar v_F\sqrt{\pi|n|})^2$ with Δ_{AB} fixed and v_F a free function of n. The red curve is a fit to theoretical models[9–11] of Fermi velocity renormalization by Coulomb interactions.

$\Delta_{AB} = 6.9$meV from the splitting of the zero energy LL (ZLL) centered at $\mu = 0$, evident in Fig. 1e where we plot $dn(\mu)/d\mu$ as determined by numerical differentiation of the $\mu(n)$ data (see also Fig. S3). Figure 1f shows $v_F(n)$, determined by fixing Δ_{AB} but allowing v_F to be a free n-dependent parameter. v_F is enhanced at low densities, consistent with past experiments[18, 19] and well fit by theoretical models of Fermi velocity renormalization[9–11], as shown by the red curve in Fig. 1f and described in the SI.

The LLs of monolayer graphene are approximately four-fold degenerate due to the spin and valley degrees of freedom, but this degeneracy is spontaneously broken at high magnetic fields via quantum Hall ferromagnetism. Fig. 2a presents $\mu(\nu)$ at B=14T across the ZLL that spans $-2 < \nu < +2$, where $\nu = 2\pi\ell_B^2 n$ is the LL filling factor. The high quality of the detector layer is crucial for achieving high experimental μ resolution, as FQH conductivity minima in the detector layer provide sensitive transducers for the sample layer chemical potential (see Fig. S4). Over large regions of density, $\mu(\nu)$ decreases as a function of ν (negative compressibility), despite the naive expectation that μ should increase monotonically with ν due to Coulomb repulsion. This is because the chemical potential measured here is actually relative to that of a classical capacitor, which subtracts off the $q = 0$ part of the Coulomb interaction $\frac{1}{2}V(q=0)n^2$. It is well understood [17, 21] that negative compressibility then arises because correlations lower the energy of quantum Hall states relative to that of a uniform charge distribution. μ jumps at each integer ν indicating incompressible integer quantum Hall states arising from the broken symmetry of the spin and valley components of the isospin. Additional jumps are observed at a series of fractional ν associated with incompressible fractional quantum Hall (FQH) states at $\nu^* = p/(2p \pm 1)$ ($p = 1, 2, 3, ...$) and $\nu^* = p/(4p \pm 1)$ (with $p = 1$ and 2)[3–5, 22]. Here $\nu^* = |\nu - \nu_0|$ indicates the filling relative to an adjacent integer filling $\nu_0 \in \mathbf{Z}$. At high B, regions (shaded in blue) around integer ν are good insulators, and so are no longer accessible at low temperatures due to the hours- or days-long equilibration time of the sample layer (see Fig. S5).

The four copies of the ZLL are nearly identical apart from an offset in chemical potential, suggesting that the LL is close to fully spin and valley polarized at this magnetic field. This is expected based on the measured value of Δ_{AB}, which splits the valley degree of freedom in the ZLL; in combination with the Zeeman energy, FQH physics is expected to be predominantly single component[15] in this regime of magnetic fields. We begin our quantitative analysis at low ν^* where electron

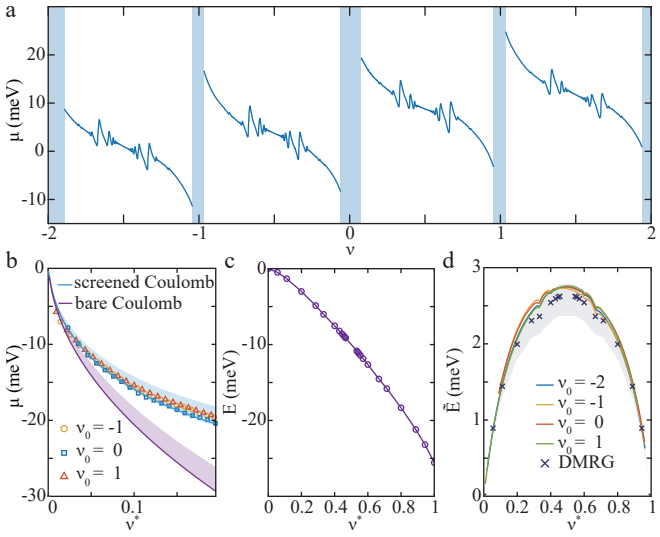

FIG. 2. **(a)** $\mu(\nu)$ within the ZLL measured at B=14T and nominal T=15mK. Blue regions indicate domains of ν where the charging time of the sample exceeds the measurement time of ∼1 second. (see Fig. S5). **(b)** μ at B=18T and nominal T=40mK for low ν^*, measured relative to $\nu = -1$ (orange), $\nu = 0$ (blue), and $\nu = 1$ (red). The cyan and purple curves are calculated μ for a Wigner crystal with screened and unscreened Coulomb interactions, respectively, taking $\epsilon_{\rm hBN} = 4.0$ and $\alpha_G = 1.85$; shaded ranges reflect uncertainty in those parameters as described in main text. The data are offset so that $\mu(\nu^*) = 0$. **(c)** Numerically calculated[20] total ground state energy of the N=0 LL after accounting for the screened Coulomb interactions. **(d)** Comparison of experimentally determined (solid lines) and numerically calculated (dark blue crosses) $\tilde{E}$. Both experimental and numerical data have a linear-in-ν^* background subtracted so that $\tilde{E}$ vanishes at integer ν^*. Data were taken at B=18T and T=40mK.

Wigner crystal phases[23, 24] are the expected ground state. In transport measurements, the Wigner crystal manifests as a low-temperature insulator that undergoes a metal-insulator transition at finite temperature due to pinning of the crystal by weak disorder, as observed in both GaAs/AlGaAs quantum wells[25] and more recently in graphene[26]. The largely classical nature of the correlations in this regime make thermodynamic modelling tractable, and quantitative agreement obtains between theory[27] and compressibility measurements in GaAs/AlGaAs quantum wells[17, 22].

Fig. 2b shows μ plotted as a function of ν^* near different integer fillings within the ZLL. For comparison, we also show theoretical calculations of μ in the Wigner crystal phase developed for the case of unscreened Coulomb interactions[24], where $\mu(\nu^*) = -1.173|\nu^*|^{1/2}E_C$. Here $E_C = \frac{e^2}{\epsilon_{\rm hBN}\ell_B}$ is the Coulomb energy. The model has only one parameter, the dielectric constant $\epsilon_{\rm hBN} = \sqrt{\epsilon^{\parallel}\epsilon^{\perp}}$, which is the geometric average of the in and out-of plane dielectric constants of the hBN substrate. $\epsilon^{\perp} = 3.0$ can be determined in situ, but $\epsilon^{\parallel}$ is not precisely known, though it is thought to be $\epsilon^{\parallel} \approx 6.6$[28]. Even accounting for uncertainty in this parameter, the model does not agree with experiment. Quantitative agreement is achieved, however, by considering the screening of the Coulomb interactions by the graphite gates, which are accounted for using standard electrostatic calculations, and by the filled Dirac sea, which we account for within the random phase approximation (RPA)[29]. RPA takes as an additional input parameter the graphene fine structure constant α_G. Still treating the electrons as a classical Wigner crystal, we numerically evaluate the Madelung-type energy for the screened interaction $V_{\rm scr}(r)$ to obtain $\mu(\nu^*)$[30]. To reflect uncertainty in the input parameters, we show a range spanning $\epsilon_{\rm hBN} \in (4.0, 4.5)$ and $\alpha_G \in (1.75, 2.2)$, in addition to reference curves for $\epsilon_{\rm hBN} = 4.0$ and $\alpha_G = 1.85$.

The screened Coulomb interaction provides an exceptionally good match to the experimental data, suggesting that no additional effects are present and that accounting for the screening is sufficient to achieve quantitative understanding of this regime. We note that based on spin-wave transmission measurements[26], spin Skyrmions appear to play a role in the Wigner solid phases near $\nu = \pm 1$. We do observe a small but systematic discrepancy between μ near even and odd integer ν in the Wigner crystal regime. This suggests that the large Zeeman energy, $E_Z \approx .03E_C$, restricts the Skyrmion size to the point where they do not generate significant corrections to μ at low ν^*.

Closer to the center of the LL, correlations become quantum in nature and even numerical calculation of μ is not tractable for arbitrary ν. However, numerical methods can accurately calculate the *total energy* per flux quantum $E(\nu)$ at many rational values of ν, as has long been the focus of exact diagonalization and density matrix renormalization group (DMRG) studies. Fig. 2c shows the ground state energy calculated using infinite DMRG[20] (iDMRG) on a circumference $L = 18\ell_B$ cylinder for a number of rational ν, assuming wave functions are restricted to a single spin and valley component and making use of the screened interaction $V_{\rm scr}$.

The calculated E is dominated by a linear background, $\mu_0\nu^*$, that is proportional to the exchange-correlation energy of the integer quantum Hall effect; the correlations underlying the FQH effect are reflected in the deviations of the calculated E from this background. In Fig. 2d, we subtract off the linear contribution by instead plotting $\tilde{E} = E - \nu^* E(\nu^* = 1)$ (Fig. 2d), which ensures $\tilde{E}(0) = \tilde{E}(1) = 0$. This can be compared with experiment by integrating $\mu(n)$, $\tilde{E}(\nu^*) = \int_0^{\nu^*}(\mu(\nu) - \mu_0)d\nu$, where μ_0 is chosen to ensure $\tilde{E}(0) = \tilde{E}(1) = 0$. To aid in fixing μ_0 accurately, the experimental data is extrapolated to integer ν by using the Wigner crystal model. Numerical and experimental data agree to within experimental uncertainty in α_G and $\epsilon_{\rm hBN}$ without additional

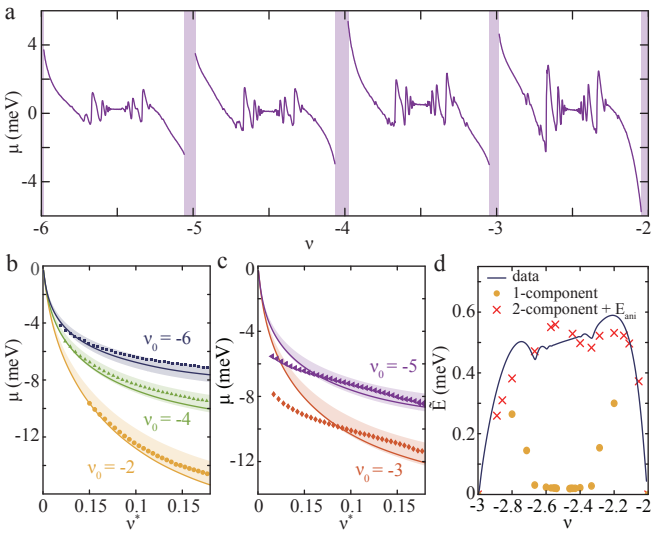

FIG. 3. **(a)** μ in the N=1 LL at T=15mK and B=13T. **(b)** μ measured near $\nu_0 = -2$, -4, and -6. Solid lines are μ calculated from the Wigner crystal model with parameters identical to those used in Fig. 2b. **(c)** μ near $\nu_0 = -3$ and -5. The solid lines showing the Wigner crystal model do not match the data, suggesting the importance of valley Merons[31] near these fillings. **(d)** Comparison of experimentally determined $\tilde{E}$ with numerical simulations for $-3 < \nu < -2$. 1-component numerical calculations underestimate the experimental result by a significant margin. Including both valley components as well as the contribution of lattice scale anisotropies as in Eq. 1 with $g_z = g_{xy} = 0.1(a/\ell_B)E_C$ can restore agreement to within $100\mu eV \approx 2.5 \times 10^{-3} E_C$.

adjustable parameters. Similarly, the measured thermodynamic gap at charge neutrality, 53meV, agrees with theoretically calculated jump in μ to within 4% [30]. These constitute remarkably good quantitative agreement for a many-body system.

Fig. 3a shows μ measured across the first excited LL, corresponding to orbital quantum number N=1 and spanning $\nu \in (-6, -2)$. In contrast to the N=0 level, both the size of the chemical potential jumps associated with FQH gaps[15] and the magnitude of the negative compressibility systematically decrease with increasing $|\nu|$. This trend arises naturally due to the nature of the screened Coulomb interaction $V_{\rm scr}$ [29]: in the ZLL, particle-hole symmetry makes the screening ν independent, but within the N=1 LL screening smoothly interpolates between the N=0 and N=2 values as the four-component LL fills. Indeed, applying this interpolation to the Wigner crystal regime near even filling factors produces an excellent quantitative match between the data and theory (Fig. 3b).

The N=1 LL and ZLL are further distinguished by the effect of the sublattice symmetry breaking Δ_{AB}, which splits the valleys in the ZLL but has negligible effect on the energies of the N=1 LL. This manifests most obviously in our data in the low-ν^* regimes around near *odd* integer filling, shown in Fig. 3c. In contrast to the comparable regimes of ν^* near even integers, and throughout the ZLL, the data are not matched by the predictions of $V_{\rm scr}$ for a single electron Wigner crystal. To understand this data, we note that tilted field magnetotransport experiments[32] find evidence for a spin polarized state at $\nu = \pm 4$ in which excitations are either single spin flips or small Skyrmions, similar to the situation at $\nu = \pm 1$ in the ZLL. At $\nu = \pm 3, \pm 5$, in contrast, activated gaps show minimal tilted field dependence, consistent with the lowest energy charged excitations being valley textures. Theoretically, the ground state of a spin-polarized but valley-unpolarized LL applicable to $\nu = \pm 3, \pm 5$ is then expected to be a solid of such valley textures[31], with resulting corrections to E and consequently to μ. Notably, the corrections to the energy will be largest when the valley textures are most extended. The observed anomalous $\mu(\nu)$ supports the idea that the low single-particle valley anisotropy in the N=1 LL stabilizes a solid of extended valley textures. This could be tested in the future by extending numerical calculations[31] of such solids to include the screened Coulomb interaction.

The multicomponent nature of the N=1 LL is further evidenced in Fig. 3d, where iDMRG simulations of a *single* component system fail to reproduce the experimentally determined $\tilde{E}$ when using the same model parameters which produce good agreement in the ZLL. Interestingly, iDMRG finds a significantly lower total energy compared to experiment. This suggests a missing contribution to the energy, since adding degrees of freedom to a variational parameter space can only lower the numerically calculated energy, increasing the discrepancy. An appealing candidate is the anisotropy of the Coulomb interactions at small length scales, which breaks the valley-$SU(2)$ symmetry and can be expected to provide corrections of $E_{ani} \sim \frac{a}{\ell_B} E_C \approx 1.75$ meV at B=13T, where $a = .246$nm is the graphene lattice constant. Though known to be important in the ZLL[1] near $\nu = 0$, evidence for short range anisotropy in the N=1 LL has been limited to the observation of a possible valley-ordered state at $\nu = 4$ for low magnetic fields[15], and they have not received much attention in the theoretical literature[33, 34].

To model their effect, we analyze the interactions which arise when projecting a short-range Hubbard-U interaction into the N=1 LL. For simplicity we assume full-spin polarization so that electrons are described by a two-component field ψ_r indexed by valley τ^z. It is convenient to express the result as the continuum interaction which would produce the same Hamiltonian if the electrons were in the N=0 LL. Taking into account the interplay of the form-factors of the N=1 LL and the sublattice

structure, we find the general form[30]

$$H_{\rm ani} = \frac{1}{2}\int d^2 r_{1/2}\left[g_z \psi^\dagger_{r_1}\tau^z\psi_{r_1}\ell_B^4\nabla^4\delta(r_1-r_2)\psi^\dagger_{r_2}\tau^z\psi_{r_2} + g_{xy}\psi^\dagger_{r_1}\tau^x\psi_{r_1}\ell_B^2\nabla^2\delta(r_1-r_2)\psi^\dagger_{r_2}\tau^x\psi_{r_2} + (x\to y)\right] \quad (1)$$

where $g_i \sim \frac{a}{\ell_B}E_c$. Note that the interactions are *derivatives* of δ-functions; in contrast, the same exercise in the ZLL would find contact interactions[34, 35]. Because the FQH effect around density $\nu^* = \frac{1}{m}$ attaches zeros $(z_i - z_j)^m$ to the inter-electron wave function, a $\nabla^{2m}\delta$ interaction effectively "turns-off" for densities below $\frac{1}{m+1}$. In the ZLL, this means the anisotropies only operate for $-1 < \nu < 1$, while in the N=1 we predict the anisotropies act for all $2 + 1/3 < \nu < 6 - 1/3$. This is indeed the region where our 1-component numerics deviate from experiment.

Treating g_z, g_{xy} as adjustable phenomenological parameters, we perform 2-component iDMRG numerics that include $H_{\rm ani}$. Fig. 3d shows the results for $g_{xy} = g_z = 0.1\frac{a}{\ell_B}E_C$, which agree with experiment to within 100 μeV, comparable to the discrepancies observed in the ZLL. In both LLs these discrepancies amount to 2×10^{-3} of the bare Coulomb energy E_C.

In conclusion, we have developed an experimental technique to measure μ to high precision in van der Waals heterostructures and applied it to high-quality graphene monolayers in the fractional quantum Hall regime, achieving remarkable agreement between experiment and numerical many-body simulations. Our technique paves the way for measuring thermodynamic quantities, such as the entropy, which may shed light on more subtle questions such as quasiparticle statistics[36].

M.P.Z. acknowledges conversations with M. Ippoliti, Z. Papic, N. Regnault, and E. Rezayi, who generously provided exact-diagonalization energies, as well as M. Metlitski. The iDMRG code used in this work was developed in collaboration with R. Mong and F. Pollmann. F.Y. and R.B acknowledge experimental assistance by H. Zhou. F.Y. acknowledges discussions with H. Polshyn and C. Tschirhart. Experimental work by F.Y., A.A.Z., R.B and A.F.Y. was supported by the National Science Foundation under DMR-1654186. Work by M.P.Z. is supported by the Army Research Office under W911NF-17-1-0323. A portion of this work was performed at the National High Magnetic Field Laboratory, which is supported by the National Science Foundation Cooperative Agreement No. DMR-1644779 and the state of Florida. K.W. and T.T. acknowledge support from the Elemental Strategy Initiative conducted by the MEXT, Japan, Grant Number JPMXP0112101001, JSPS KAKENHI Grant Number JP20H00354 and the CREST(JPMJCR15F3), JST. A.F.Y. acknowledges the support of the David and Lucile Packard Foundation.

* andrea@physics.ucsb.edu

[1] C. Dean, P. Kim, J. I. A. Li, and A. Young, in Fractional Quantum Hall Effects: New Developments (World Scientific, Singapore, 2020) pp. 317–375.

[2] J. Martin, N. Akerman, G. Ulbricht, T. Lohmann, J. H. Smet, K. von Klitzing, and A. Yacoby, Nature Physics **4**, 144 (2008).

[3] B. E. Feldman, B. Krauss, J. H. Smet, and A. Yacoby, Science **337**, 1196 (2012).

[4] B. E. Feldman, A. J. Levin, B. Krauss, D. A. Abanin, B. I. Halperin, J. H. Smet, and A. Yacoby, Physical Review Letters **111**, 076802 (2013).

[5] A. A. Zibrov, E. M. Spanton, H. Zhou, C. Kometter, T. Taniguchi, K. Watanabe, and A. F. Young, Nature Physics **14**, 930 (2018).

[6] K. Lee, B. Fallahazad, J. Xue, D. C. Dillen, K. Kim, T. Taniguchi, K. Watanabe, and E. Tutuc, Science **345**, 58 (2014).

[7] B. Hunt, J. D. Sanchez-Yamagishi, A. F. Young, M. Yankowitz, B. J. LeRoy, K. Watanabe, T. Taniguchi, P. Moon, M. Koshino, P. Jarillo-Herrero, and R. C. Ashoori, Science **340**, 1427 (2013).

[8] F. Amet, J. R. Williams, K. Watanabe, T. Taniguchi, and D. Goldhaber-Gordon, Physical Review Letters **110**, 216601 (2013).

[9] J. González, F. Guinea, and M. A. H. Vozmediano, Physical Review B **59**, R2474 (1999), publisher: American Physical Society.

[10] S. Das Sarma, E. H. Hwang, and W.-K. Tse, Physical Review B **75**, 121406 (2007), publisher: American Physical Society.

[11] M. Polini, R. Asgari, Y. Barlas, T. Pereg-Barnea, and A. H. MacDonald, Solid State Communications Exploring graphene, **143**, 58 (2007).

[12] J. Yan and M. S. Fuhrer, Nano Lett. **10**, 4521 (2010).

[13] Y. Zhao, P. Cadden-Zimansky, F. Ghahari, and P. Kim, Physical Review Letters **108**, 106804 (2012).

[14] M. J. Zhu, A. V. Kretinin, M. D. Thompson, D. A. Bandurin, S. Hu, G. L. Yu, J. Birkbeck, A. Mishchenko, I. J. Vera-Marun, K. Watanabe, T. Taniguchi, M. Polini, J. R. Prance, K. S. Novoselov, A. K. Geim, and M. Ben Shalom, Nature Communications **8**, 14552 (2017).

[15] H. Polshyn, H. Zhou, E. M. Spanton, T. Taniguchi, K. Watanabe, and A. F. Young, Physical Review Letters **121**, 226801 (2018).

[16] Y. Zeng, J. Li, S. Dietrich, O. Ghosh, K. Watanabe, T. Taniguchi, J. Hone, and C. Dean, Physical Review Letters **122**, 137701 (2019).

[17] J. P. Eisenstein, L. N. Pfeiffer, and K. W. West, Phys. Rev. Lett. **68**, 674 (1992).

[18] D. C. Elias, R. V. Gorbachev, A. S. Mayorov, S. V. Morozov, A. A. Zhukov, P. Blake, L. A. Ponomarenko, I. V. Grigorieva, K. S. Novoselov, F. Guinea, and A. K. Geim, Nature Physics **7**, 701 (2011).

[19] J. Chae, S. Jung, A. F. Young, C. R. Dean, L. Wang, Y. Gao, K. Watanabe, T. Taniguchi, J. Hone, K. L. Shepard, P. Kim, N. B. Zhitenev, and J. A. Stroscio, Physical Review Letters **109**, 116802 (2012).

[20] M. P. Zaletel, R. S. K. Mong, F. Pollmann, and E. H. Rezayi, Physical Review B **91**, 045115 (2015).

[21] G. Fano, F. Ortolani, and E. Colombo, Physical Review B **34**, 2670 (1986), publisher: American Physical Society.

[22] J. P. Eisenstein, L. N. Pfeiffer, and K. W. West, Phys. Rev. B **50**, 1760 (1994).

[23] P. K. Lam and S. M. Girvin, Physical Review B **30**, 473 (1984).

[24] D. Levesque, J. J. Weis, and A. H. MacDonald, Physical Review B **30**, 1056 (1984).

[25] V. J. Goldman, M. Santos, M. Shayegan, and J. E. Cunningham, Physical Review Letters **65**, 2189 (1990).

[26] H. Zhou, H. Polshyn, T. Taniguchi, K. Watanabe, and A. F. Young, Nature Physics (2019), 10.1038/s41567-019-0729-8.

[27] L. Bonsall and A. A. Maradudin, Physical Review B **15**, 1959 (1977), publisher: American Physical Society.

[28] R. Geick, C. H. Perry, and G. Rupprecht, Physical Review **146**, 543 (1966).

[29] K. Shizuya, Phys. Rev. B **75** (2007).

[30] See online Supplementary Information.

[31] R. Côté, J.-F. Jobidon, and H. A. Fertig, Physical Review B **78**, 085309 (2008), publisher: American Physical Society.

[32] A. F. Young, C. R. Dean, L. Wang, H. Ren, P. Cadden-Zimansky, K. Watanabe, T. Taniguchi, J. Hone, K. L. Shepard, and P. Kim, Nature Physics **8**, 550 (2012).

[33] J. Alicea and M. P. A. Fisher, Phys. Rev. B **74**, 075422 (2006).

[34] M. Kharitonov, Phys. Rev. B **85**, 155439 (2012).

[35] I. Sodemann and A. MacDonald, Physical Review Letters **112**, 126804 (2014).

[36] N.R. Cooper and A. Stern, Physical Review Letters **102**, 176807 (2009).

[37] J. Zhu, H. L. Stormer, L. N. Pfeiffer, K. W. Baldwin, and K. W. West, Physical Review B **61**, R13361 (2000), publisher: American Physical Society.

[38] E. Tutuc, R. Pillarisetty, S. Melinte, E. P. De Poortere, and M. Shayegan, Physical Review B **68**, 201308 (2003), publisher: American Physical Society.

[39] W. Pan, J. L. Reno, and J. A. Simmons, Physical Review B **71**, 153307 (2005), publisher: American Physical Society.

[40] S. Misra, N. C. Bishop, E. Tutuc, and M. Shayegan, Physical Review B **78**, 035322 (2008), publisher: American Physical Society.

[41] A. Usher and M. Elliott, Journal of Physics: Condensed Matter **21**, 103202 (2009).

[42] N. Ruhe, G. Stracke, C. Heyn, D. Heitmann, H. Hardtdegen, T. Schäpers, B. Rupprecht, M. A. Wilde, and D. Grundler, Physical Review B **80**, 115336 (2009).

[43] L. H. Ho, L. J. Taskinen, A. P. Micolich, A. R. Hamilton, P. Atkinson, and D. A. Ritchie, Physical Review B **82**, 153305 (2010).

[44] J. Pollanen, J. P. Eisenstein, L. N. Pfeiffer, and K. W. West, Physical Review B **94**, 245440 (2016).

[45] I. F. Herbut, Phys. Rev. B **75** (2007).

[46] J. Jung and A. H. MacDonald, Phys. Rev. B **80** (2009).

[47] K. Nomura, S. Ryu, and D.-H. Lee, Phys. Rev. Lett. **103** (2009).

[48] D. V. Khveshchenko, Phys. Rev. Lett. **87** (2001).

[49] A. F. Young, J. D. Sanchez-Yamagishi, B. Hunt, S. H. Choi, K. Watanabe, T. Taniguchi, R. C. Ashoori, and P. Jarillo-Herrero, Nature **505**, 528 (2014).